

The Impact of Run-Time Variability on Side-Channel Attacks Targeting FPGAs

Davide Galli[✉], Adriano Guarisco, William Fornaciari[✉], Matteo Matteucci[✉], Davide Zoni[✉]
DEIB,

Politecnico di Milano,
 Milano, Italy,

{davide.galli, william.fornaciari, matteo.matteucci, davide.zoni}@polimi.it, adriano.guarisco@mail.polimi.it

Abstract—To defeat side-channel attacks, many recent countermeasures work by enforcing random run-time variability to the target computing platform in terms of clock jitters, frequency, and voltage scaling, and phase shift, also combining the contributions from different actuators to maximize the side-channel resistance of the target. However, the robustness of such solutions seems strongly influenced by several hyper-parameters for which an in-depth analysis is still missing.

This work proposes a fine-grained dynamic voltage and frequency scaling actuator to investigate the effectiveness of recent desynchronization countermeasures with the goal of highlighting the link between the enforced run-time variability and the vulnerability to side-channel attacks of cryptographic implementations targeting FPGAs. The analysis of the results collected from real hardware allowed for a comprehensive understanding of the protection offered by run-time variability countermeasures against side-channel attacks.

Index Terms—DVFS, FPGA, run-time variability, side-channel attacks

I. INTRODUCTION

Side-channel attacks (SCA) represent one of the most prominent security threats against modern cryptographic implementations. Starting from the introduction of power [1] and electromagnetic [2] analysis, the design of countermeasures has become an increasingly important topic. Notably, side-channel countermeasures can be organized into two categories: masking and hiding. Masking countermeasures degrade the side-channel signal-to-noise ratio (SNR) by splitting the sensitive intermediate values into different shares that are computed independently. Hiding countermeasures degrade the side-channel SNR by increasing the noise component. Unlike masking solutions, hiding countermeasures do not offer provable security, while the achievable low resource overhead fueled extensive research [3]–[5]. Trace desynchronization represents a relatively cheap and, thus, widely employed hiding countermeasure that works by invalidating the common attack hypothesis for which the collected traces should be time-aligned to each other. Several proposed trace desynchronization techniques leverage the dynamic voltage and frequency scaling (DVFS) actuator to randomly change the operating frequency and voltage of the target computing platform at run-time [3], [6], [7]. Considering deep sub-micron technology

nodes, clock jitter represents a process variability effect that has been observed to contribute severely to trace desynchronization [8], [9]

Literature demonstrated the effectiveness of desynchronization countermeasures and highlighted how the attack success rate degrades with the increase of the desynchronization [10]. However, there needs to be a clear understanding of the hyperparameters and their values to maximize the side-channel resistance of desynchronization countermeasures.

Contributions - Considering modern FPGAs, this work investigates the link between the trace desynchronization and the side-channel attack’s success rate, leveraging the Pearson correlation coefficient (ρ) quality metric, making two contributions to the state of the art.

- *Random DVFS module* - We introduce a hardware module targeting AMD Xilinx FPGAs that performs dynamic and fine-grained operating voltage, frequency, and phase scaling. Our solution offers fast temporal dynamics in the order of tens of microseconds, a fine-grained scaling of the operating parameters, and a continuous operating mode even during voltage and frequency changes.
- *Real hardware experimental analysis* - We perform an extensive experimental campaign targeting multiple AMD Xilinx Artix-7 FPGA instances to assess the effects of trace desynchronization through random DVFS, taking into account the phase shift and inter-chip process variability. The findings are threefold. First, analog parts in the DVFS actuator can hinder the attack by introducing low-dynamic components into the power consumption. However, using a high-pass filter restores most of the side-channel vulnerabilities. Second, inter-chip FPGA variability is not sufficient to hide side-channel leakages. Third, frequency scaling is the most effective hiding technique of the evaluated ones. The robustness of trace desynchronization techniques improves with the distance between operating frequencies rather than depending on the number of frequencies used, as suggested in [3].

II. FINE-GRAINED RANDOM DVFS ARCHITECTURE

This section presents the random dynamic voltage and frequency scaling architecture (*rDVFS*) to perform fast and fine-grained actuation.

This work was supported by the European Union’s Chips Joint Undertaking (Chips JU) program under grant agreement No. 101112274 (ISOLDE).

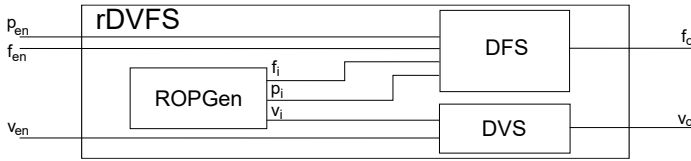


Fig. 1: Architectural view of the proposed random dynamic voltage and frequency scaling (*rDVFS*).

Figure 1 depicts the high-level view of the *rDVFS* architecture. The *rDVFS* receives three independent control signals, i.e., f_{en} , p_{en} , and v_{en} , used to selectively enable the random scaling of the clock frequency (f_{en}), the clock phase (p_{en}), and the operating voltage (v_{en}), and outputs the generated clock (f_o) and the operating voltage (v_o) signals. Notably, the control signals, i.e., f_{en} , p_{en} , and v_{en} , allow to selectively force the actuation of a portion or the entire random operating point. The *rDVFS* architecture is made of three sub-modules: *ROPGen*, *DFS*, and *DVS*.

The rest of this section details the architecture of the *ROPGen* and the *DFS* modules, which represent the on-chip components of the random DVFS actuator. Current FPGAs do not offer on-chip DVS actuators, and thus, we exploit the *DVS* of the reference board leveraging the SPI/I2C protocol.

Random operating point generator (ROPGen) - The module implements a free-running true random number generator (TRNG) [11] to address memories containing the configurations for each parameter, i.e., clock frequency, clock phase, and operating voltage. The module’s output consists of the random operating point in terms of frequency, phase, and voltage. The three memories are independently accessed, and the content of the memories is configured at design time according to the feasibility requirements described in the technical specification documents of the considered hardware components [12]. The design-time configuration script allows users to specify boundaries and step increments for frequency and operating voltage, automatically generating the RTL description for correctly instantiated memories. Even if the architecture is generic, we allow up to 1024 frequency configurations, 8 clock phase configurations, and 128 operating voltage values. The limited number of phase configurations arises from the practical challenges of achieving rapid phase shifts for large phase values using the Xilinx MMCM [13]. To this end, we obtained large clock phase shifts by serializing multiple small phase shift actuations.

Dynamic Frequency Scaling (DFS) actuator - Figure 2 overviews the architecture of the *DFS* actuator. The module takes as inputs the clock frequency (f_i) and the clock phase (p_i), as well as two control signals (f_{en} and p_{en}) to independently enable the actuation of the two operating points. The *DFS* outputs the generated clock signal (f_o). The architecture of *DFS* is organized in three parts: *i*) the storage element (*BRAM36*) contains the configuration parameters for the frequency scaling, *ii*) the pair of Mixed-Mode Clock Modules, i.e., *MMCM_A* and *MMCM_B*, represents

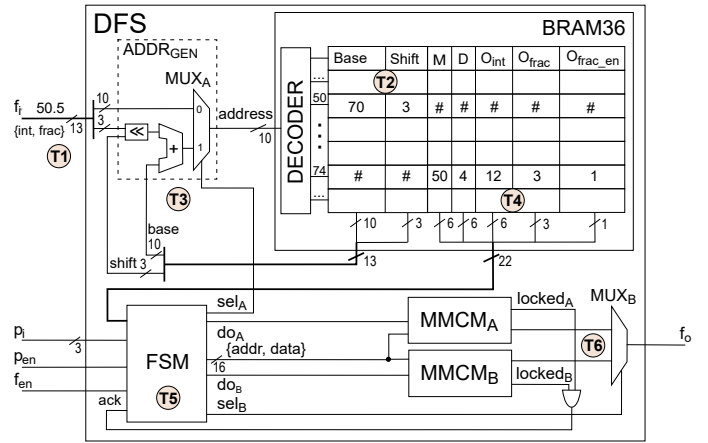


Fig. 2: Architectural view of the proposed dynamic frequency scaling (*DFS*) actuator.

the actual generators of the clock signal (f_o), and *iii*) the finite-state machine (*FSM*) and the related address generator logic (*ADDR_{GEN}*) implement the protocol to perform the frequency and phase scaling.

The proposed *DFS* leverages two MMCMs to avoid the clock-gating effect during the reconfiguration of the clock signal. The master MMCM keeps generating the current clock signal while the slave MMCM undergoes reconfiguration. After reconfiguration, their roles switch, ensuring a truly dynamic frequency scaling actuator.

The *FSM* module implements the protocol to reconfigure the clock frequency and phase dynamically. Inputs consist of clock frequency (f_i) and clock phase (p_i), control signals for frequency (f_{en}) and phase (p_{en}) reconfiguration, and a signal monitoring the locked status of both MMCMs (*ack*). Frequency and phase can be reconfigured independently. The *ack* signal prevents a new reconfiguration while the previous one is still in progress.

The *FSM* configures the registers in the memory-mapped MMCM interfaces to change the clock frequency and phase dynamically. Notably, the phase shift can be actuated by directly writing the correct MMCM memory-mapped register, while the frequency reconfiguration involves multiple MMCM registers for which the corresponding values are obtained from *BRAM36*. Considering the design of this flexible architecture and the limitations of the Xilinx MMCMs, the *BRAM36* can store up to 1024 clock frequency configurations ranging from 5 MHz to 800 MHz due to MMCM feasibility constraints, with a minimum step of 0.125 MHz.

To further illustrate the proposed solution, consider reconfiguring the frequency of 50.5 MHz (see T1-T6 in Figure 2). Starting from the input frequency value $f_i = 50.5 \text{ MHz}$ (T1), the integer part initiates the first access to *BRAM36* (T2). From the obtained record, the *Base* and the *Shift* fields are used to make the address for the second access to *BRAM36* containing the clock frequency configuration for f_i . In particular, the configuration to obtain an operating frequency equal to 50.5 is stored at line 74. The configuration values *M*, *D*,

O_{int} , O_{frac} , $O_{frac_{en}}$ at line 74, are driven to the FSM to configure the slave MMCM registers ($T5$). Once the slave MMCM sets its *locked* signal, the FSM drives sel_B to flip the role of the MMCMs and to propagate the new frequency through f_o ($T6$).

III. EXPERIMENTAL EVALUATION

This section discusses the experimental results with the final goal of highlighting the trace desynchronization parameters that mainly affect the protection against side-channel attacks (SCA).

A. Experimental setup

Hardware and software setup - We implemented the proposed random DVFS into the NewAE CW305 board [14]. The board features an FPGA socket that allows changing the mounted FPGA chip. We employed a 32-bit RISC-V System-on-Chip [11], [15] as the reference computing platform executing an unprotected software implementation of the AES-128 cryptosystem. The power traces were collected from the 20 dB-amplified output of the CW305 board using a Picoscope 5244d oscilloscope, sampling at 250 Msamples/s, with a resolution of 12 bits. The setup features a dedicated hardware signal from the computing platform to trigger the oscilloscope at the beginning of each encryption. To prevent measurement pollution due to the ringing effects derived from the assertion of the trigger signal, we inserted a slight delay between the trigger assertion and the actual beginning of the encryption.

Configurations - Our analysis considered the trace desynchronization achieved by scaling each parameter, i.e., clock frequency, clock phase, operating voltage, and different FPGA chips, in isolation. Notably, our *rDVFS* is enabled for the entire encryption. Thus, a new configuration is requested as soon as one is locked. To this end, each encryption observes multiple clock frequency and voltage reconfigurations.

For each configuration, Table I reports the boundary values and the step of the considered parameter.

Attack methodology - To assess the side-channel vulnerability, we utilized correlation power analysis (CPA) and template attack (TA), focusing on the $SEOX$ operation in the initial AES round. CPA is performed up to 100k traces on the *train* chip of Table I, while the template has been trained considering 1k traces per key value.

Multiple attacks were executed for each scenario and method. The primary attack used unprocessed traces, while subsequent ones incorporated post-processing, specifically sample aggregation and a high-pass filter (HPF) with a 125 kHz cutoff to eliminate low-frequency signal components.

B. Quality metrics

Security results are discussed in terms of two quality metrics, *i*) Pearson Correlation Coefficient ρ between the power traces and the power estimation is used as an equivalent representation of SNR, *ii*) Guessing entropy GE is used to evaluate the effectiveness of the TA, defined as the average

TABLE I: Values in terms of operating voltage, clock frequency, clock phase shift, and used chip, for each experimental configuration.

	ID	Num. of steps	Voltage [V]	Frequency [MHz]	Phase [°]	Chip Train (Attack)
Chip	C1	1	1	50	0	Artix-7 100 (Artix-7 35)
	C2	1	1	50	0	Artix-7 35 (Artix-7 100)
DVS	V1	3	[0.99; 1.01] step 0.01	50	0	Artix-7 100 (Artix-7 100)
	V2	2	{0.75, 1.05}	50	0	
	V3	11	[0.75; 1.05] step 0.03	50	0	
DPS	P1	9	1	50	[0; 30] step 3.75	
DFS	F1	9	1	[38.375; 39.5] step 0.125	0	
	F2	7	1	[30; 65] step 5.0	0	
	F3	6	1	[25; 75] step 10.0	0	
	F3 ₁₂₅	401	1	[25; 75] step 0.125	0	

TABLE II: ρ , CPA, and TA comparison between all the configurations, both with and without filtering the traces and aggregating up to 1k samples (\checkmark if $GE = 1$).

	ID	Aggregate n samples	ρ		CPA		TA	
			Raw	HPF	Raw	HPF	Raw	HPF
Synch		1	0.419	0.388	200	200	\checkmark	\checkmark
		100	0.587	0.555	200	200	\checkmark	\checkmark
		1k	0.557	0.360	200	500	\checkmark	\checkmark
Chip	C1	1	0.419	0.388	200	200	\checkmark	\checkmark
	C2	1	0.353	0.402	200	200	\checkmark	\checkmark
DVS	V1	1	0.428	0.435	200	200	\checkmark	\checkmark
	V2	1	0.089	0.326	10k	500	\times	\checkmark
	V3	1	0.102	0.335	10k	500	\times	\checkmark
DPS	P1	1	0.191	0.185	200	500	\checkmark	\checkmark
		100	0.220	0.202	200	500	\checkmark	\checkmark
		1k	0.170	0.089	500	1k	\checkmark	\checkmark
DFS	F1	1	0.046	0.033	\times	\times	\times	\times
		100	0.215	0.184	5k	5k	\checkmark	\checkmark
		1k	0.252	0.166	5k	5k	\checkmark	\checkmark
	F2	1	0.033	0.034	\times	\times	\times	\times
		100	0.032	0.031	\times	\times	\times	\times
		1k	0.031	0.018	\times	\times	\times	\times
	F3	1	0.040	0.044	\times	\times	\times	\times
		100	0.029	0.031	\times	\times	\times	\times
		1k	0.027	0.024	\times	\times	\times	\times
	F3 ₁₂₅	1	0.035	0.033	\times	\times	\times	\times
		100	0.031	0.028	\times	\times	\times	\times
		1k	0.028	0.024	\times	\times	\times	\times

rank position of the correct key among all possible key guesses.

C. Experimental results

Table II summarizes the experimental results. The *Synch* configuration reports the quality metrics for the reference design with no desynchronization. For each scenario (*ID*), results are reported in terms of ρ values, number of traces to recover all 16 bytes using *CPA*, and effectiveness of *TA*. For each scenario, results are reported with and without the HPF and different levels of aggregation. Notably, the aggregation can resynchronize the traces by averaging continuous samples at the risk of a decreased SNR.

Inter-chip variability and clock phase - The inter-chip process variability on AMD Xilinx Artix-7 FPGAs is too small to prevent an attack using a model trained on one FPGA instance to target another (see $C1$ and $C2$ in Table II). Notably, such results contrast those reported from analyzing the process variability targeting ASIC [16], thus motivating the need for separate investigations. Similarly, dynamic phase shift provokes a negligible degradation in the side-channel attacks' success (see DPS in Table II).

Operating voltage - The attack's success rate diminishes as the operating voltage range increases. Considering the Raw traces, ρ lowers from 0.428 in $V1$ to 0.102 in $V3$, thus highlighting the benefit of the voltage scaling. Conversely, using a high-pass filter on the DVS collected traces shows a non-negligible improvement of ρ , as well the efficacy of CPA and TA . The motivation behind such behavior is the low-frequency component over-imposed by the actuators on the power consumption. The scaling actuations provoke severe oscillations in the side-channel signal, thus reducing ρ values and the effectiveness of the various SCAs. However, the low dynamic of the over-imposed signal can be removed by applying a high-pass filter to the measured traces.

Clock frequency - Experimental results confirm the effectiveness of dynamic frequency scaling as desynchronization countermeasures. Similarly to DVS, the side-channel attacks degrade with the increase in the range of the DFS actuator. For example, $F1$ and $F3$ employ a frequency range of [38.375 – 39.5] MHz and [25 – 75] MHz, respectively. The CPA and TA results confirm that $F3$ makes the attacks harder than $F1$.

Considering the employed post-processing techniques, the high-pass filter (HPF) fails to improve the SCA. In contrast, aggregation severally improves the side-channel attacks. For example, aggregating 100 samples allows CPA to succeed for all key bytes with $5k$ traces in the $F1$ scenario (see Table II). Notably, none of the considered attacks succeed in the $F2$ and $F3$ scenarios regardless of the employed post-processing technique, thus highlighting the effectiveness of severe trace desynchronization against SCA.

At last, we analyzed the effect of using a large variety of dynamic frequencies to improve the side-channel resistance as proposed in [3]. The frequency scenario $F3_{125}$ considers the step between two consecutive operating frequencies equal to 125 kHz. In addition, $F1$ mimics the effect of clock jitter. Our experimental results demonstrate that using a high number of frequencies offers negligible improvements to the side-channel resistance.

IV. CONCLUSIONS

This paper investigated the effectiveness of trace desynchronization techniques using DVFS targeting AMD Xilinx Artix-7 FPGAs. By presenting a random, fine-grained DVFS actuator, we provided a vast experimental campaign demonstrating that dynamic phase shift is ineffective as a desynchronization countermeasure. Moreover, the effect of

dynamic voltage scaling is mainly due to the analog parts of the actuator and can be defeated through a high-pass filter. Dynamic frequency scaling (DFS) emerged as the most effective technique to implement effective desynchronization. In particular, the resistance against SCA improves as the range of frequency scaling increases. Such consideration highlights a critical trade-off between security and performance, i.e., using DFS for security requires a high variability in operating frequencies, thus reducing the overall performance and the execution time predictability.

REFERENCES

- [1] P. C. Kocher, J. Jaffe, and B. Jun, "Differential power analysis," in *Proceedings of the 19th Annual International Cryptology Conference on Advances in Cryptology*, ser. CRYPTO '99. Berlin, Heidelberg: Springer-Verlag, 1999, pp. 388–397.
- [2] J. Heyszl, S. Mangard, B. Heinz, F. Stumpf, and G. Sigl, "Localized electromagnetic analysis of cryptographic implementations," in *Topics in Cryptology – CT-RSA 2012*, O. Dunkelman, Ed. Berlin, Heidelberg: Springer Berlin Heidelberg, 2012, pp. 231–244.
- [3] B.-A. Dao, T.-T. Hoang, A.-T. Le, A. Tsukamoto, K. Suzuki, and C.-K. Pham, "Correlation power analysis attack resisted cryptographic risc-v soc with random dynamic frequency scaling countermeasure," *IEEE Access*, vol. 9, pp. 151993–152014, 2021.
- [4] G. Chiari, D. Galli, F. Lattari, M. Matteucci, and D. Zoni, "A deep-learning technique to locate cryptographic operations in side-channel traces," in *2024 Design, Automation & Test in Europe Conference & Exhibition (DATE)*, 2024, pp. 1–6.
- [5] D. Galli, G. Chiari, and D. Zoni, "Hound: Locating cryptographic primitives in desynchronized side-channel traces using deep-learning," 2024. [Online]. Available: <https://arxiv.org/abs/2408.06296>
- [6] S. Yang, W. Wolf, N. Vijaykrishnan, D. Serpanos, and Y. Xie, "Power attack resistant cryptosystem design: a dynamic voltage and frequency switching approach," in *Design, Automation and Test in Europe*, 2005, pp. 64–69 Vol. 3.
- [7] B. Hettwer, K. Das, S. Leger, S. Gehrler, and T. Güneysu, "Lightweight side-channel protection using dynamic clock randomization," in *2020 30th International Conference on Field-Programmable Logic and Applications (FPL)*, 2020, pp. 200–207.
- [8] E. Cagli, C. Dumas, and E. Prouff, "Convolutional Neural Networks with Data Augmentation against Jitter-Based Countermeasures," in *Cryptographic Hardware and Embedded Systems - CHES 2017 - 19th International Conference*, Taipei, Taiwan, Sep. 2017.
- [9] L. Masure, N. Belleville, E. Cagli, M.-A. Cornélie, D. Couroussé, C. Dumas, and L. Maingault, "Deep learning side-channel analysis on large-scale traces - a case study on a polymorphic aes," *Cryptology ePrint Archive*, Paper 2020/881, 2020. [Online]. Available: <https://eprint.iacr.org/2020/881>
- [10] R. Benadjila, E. Prouff, R. Strullu, E. Cagli, and C. Dumas, "Deep learning for side-channel analysis and introduction to ascad database," *Journal of Cryptographic Engineering*, vol. 10, 06 2020.
- [11] D. Galli, A. Galimberti, W. Fornaciari, and D. Zoni, "On the effectiveness of true random number generators implemented on fpgas," in *International Conference on Embedded Computer Systems*. Springer, 2022, pp. 315–326.
- [12] AMD Xilinx, *Artix-7 FPGAs Data Sheet: DC and AC Switching Characteristics*, DS181, 2022.
- [13] AMD Xilinx and J. Tatsukawa, *MMCM and PLL Dynamic Reconfiguration*, XAPP888, 2019.
- [14] NewAE Technology Inc., "Cw305 artix fpga target," 2018. [Online]. Available: <https://rtfm.newae.com/Targets/CW305%20Artix%20FPGA>
- [15] L. Denisov, A. Galimberti, D. Cattaneo, G. Agosta, and D. Zoni, "Design-time methodology for optimizing mixed-precision cpu architectures on fpga," *Journal of Systems Architecture*, vol. 155, p. 103257, 2024. [Online]. Available: <https://www.sciencedirect.com/science/article/pii/S1383762124001942>
- [16] M. Renaud, F.-X. Standaert, N. Veyrat-Charvillon, D. Kamel, and D. Flandre, "A formal study of power variability issues and side-channel attacks for nanoscale devices," in *Annual International Conference on the Theory and Applications of Cryptographic Techniques*. Springer, 2011, pp. 109–128.